25 March 1986

JETSET: Physics at LEAR with an Internal Gas Jet Target and an Advanced General Purpose Detector

G.Bassompierre[1], R.K.Bock[2], A.Buzzo[5], M.Dameri[5], T.Fearnley[7], J.Franz[3], M.Gazzaly[10], N.Hamann[3], T.Johansson[8], E.Khan-Aronsen[7], K.Kilian[6], J.Kirkby[2], K.Kirsebom[7], K.Kuroda[1], A.Kylling[7], F.Levrero[4], A.Lundby[2], M.Macri[5], M.Marinelli[4], L.Mattera[4], B.Mouellic[2], B.A.Nielsen[7], W.Oelert[6], Y.Onel[4], B.Osculati[5], G.Pauletta[9], M.G.Pia[5], M.Poulet[1], E.Rössle[3], A.Santroni[5], H.Schmitt[3], B.Stugu[7], S.Terreni[4], F.Tommasini[5]

ABSTRACT

We argue the importance of installing at LEAR an internal gas jet target together with a powerful detection system. We discuss an advanced detector which will offer large acceptance and complete information on charged and neutral tracks, in its final implementation. We propose here a phase 1 realisation of this detector which will allow us to carry out a set of fundamental experiments at LEAR during the early operation of ACOL. They comprise studies of $\phi\phi$ and $K^0_S K^0_S$ production, on both unpolarized and polarized hydrogen targets, over the range $1960 < \sqrt{s} < 2400$ MeV.

[1] LAPP Annecy, France
[2] CERN, European Laboratory for Particle Physics, Geneva, Switzerland
[3] Freiburg University, FRG
[4] Geneva University, Switzerland
[5] Genova University and INFN, Italy
[6] Kernforschungsanlage Jülich, FRG
[7] Oslo University, Norway
[8] Uppsala University, Sweden
[9] University of Texas, Austin, USA, and INFN Trieste, Italy
[10] University of Minnesota, Minneapolis, USA

1. INTRODUCTION

We present here a proposal based on the ideas outlined in the memorandum M252 to the PSCC [1]. We summarize briefly our general arguments for the outstanding physics potential of an internal gas jet target at LEAR:

- Maximum luminosity. About 100 events/nbarn can be collected daily for the target thickness and density proposed, assuming 10^{10} circulating antiprotons. The luminosities are at least one order of magnitude larger than can be obtained by in-flight experiments with extracted beams.
- The narrow energy spread of the circulating beam. At LEAR the momentum spread $\Delta p/p < 10^{-3}$ translates into $\Delta(\sqrt{s}) < 1$MeV over the full range of $\sqrt{s}$. This feature, combined with the facility of changing beam energy rapidly during data taking, is a major asset in resonance searches and associated s-channel studies.
- The provision of a polarized proton target. This is an essential tool in understanding final state quantum numbers.
- Experimental simplicity. The small interaction volume (< 1 cm^3) simplifies the experimental apparatus, the trigger, and the analysis. The internal target operation in addition disposes of all non-interacting beam tracks.

Gas jet targets in storage rings have already shown to be a powerful tool for experiments in particle physics [2]. The interest in an internal jet target at LEAR has been pointed out by P.Dalpiaz [3], K.Kilian [4], U.Gastaldi and R.Klapisch [5]. The technical implications of such a target on the machine, which have been presented by D.Möhl [6], are discussed below.

It is our intention ultimately to surround the gas jet target with a general-purpose large-acceptance detector of advanced technology, thus taking full advantage of the unique capabilities of such a target. In the final detector configuration, precise charged track measurements will be made in a high magnetic field, complete particle identification will be possible in RICH counters, and electromagnetic calorimeters will provide high-resolution measurements of neutral particles such as π^0, η, and η'. The physics programme that can be envisaged with such a detector is outstanding. Two aspects deserve special mention:

- Systematic searches for resonances in the s-channel, with final states containing hidden strangeness like ϕ, η or η', or strange particles. Of particular interest are the final states $\phi\phi$, ϕKK, 4K, $\Lambda\bar{\Lambda}$, $\eta\eta'$, $\phi\eta$, K*K*, and KKη. The cross sections for such reactions, inasmuch as they are known, are small, at the μb level.
- Lower-mass resonances produced in association with other particles. These searches place demanding requirements on detector resolution and particle identification. Such particles are produced with similar luminosities in the gas jet target and by extracted beams stopping in external targets. Our detector, with the important assets of its polarized target, high resolution, and independent systematics, can be seen as an alternative device for cross-checking results found in LEAR experiments with extracted beams.

We should also underline that this detector is an obvious candidate for operating in a colliding beam mode at LEAR, should such a programme become available in the future.

It is the objective of this proposal to concentrate on a **phase 1** detector and physics programme. As phase 1 detector, in agreement with our collaboration's present strength, we propose to build

- an inner tracking device of high resolution,
- a fast RICH with K/π discrimination in the MHz range,
- a system of trigger scintillation counters.

The phase 1 physics programme will focus on measurements of the differential cross sections and polarization parameters of the two exclusive channels $\bar{p}p \to \phi\phi \to K^-K^-K^+K^-$ and $\bar{p}p \to K^0_S K^0_S \to \pi^+\pi^-\pi^+\pi^-$.

Measurements will be made in the beam momentum range 600 − 1900 MeV/c. In a first step, a molecular hydrogen jet will be installed to operate with maximum luminosity. Subsequently, the production stage will be replaced, and measurements will be repeated with a polarized atomic hydrogen beam of chosen spin orientation.

2. THE PHASE 1 PHYSICS PROGRAMME

We propose to measure the differential cross- section $d\sigma/d\Omega$ and the polarization parameter P of the two exclusive channels

$$\bar{p}p \rightarrow \phi\phi \rightarrow K^+K^-K^+K^-$$
$$\bar{p}p \rightarrow K^0_S K^0_S \rightarrow \pi^+\pi^-\pi^+\pi^-$$

at about 12 different energies in the range $1960 < \sqrt{s} < 2400$ MeV.

After completion of these initial studies, which include the first measurement of the $\bar{p}p \rightarrow \phi\phi$ cross section, we will be able to determine the optimum strategy for the next stage of our experiment: a search for s-channel resonances due to gluonic or other types of new particles.

2.1 $\bar{p}p \rightarrow \phi\phi$

This reaction (threshold at $\sqrt{s} = 2040$ MeV) represents a fundamental process in the framework of QCD, since it provides information on the mechanisms of the complete quark-antiquark annihilation of the $\bar{p}p$ system into $s\bar{s}$ quarks. It is an OZI-suppressed channel (i.e. no possible quark line connection between initial and final state), and the intermediate state consists of gluons, as it does in hadronic production of $c\bar{c}$. Fig 2.1.a sketches this process in the s channel. The series of quantum numbers accessible to both $\bar{p}p$ and $\phi\phi$ are $J^{PC} = 0^{-+}, 0^{++}, 1^{++}, 2^{-+}, 2^{++}, 3^{+-}, 4^{-+}, \ldots$, with a pure isospin I = 0. In the picture of a reaction mediated by pure gluons, the above quantum numbers can be carried by two massless gluons, with the exception of the 1^{++} intermediate state, for which three gluons are necessary. Practically, we can imagine the $\bar{p}p \rightarrow \phi\phi$ reaction as a two-gluon factory, which may be a continuum of gluons producing new flavours of quarks and antiquarks (Fig 2.1.a), or which may pass through resonant states for some values of $\sqrt{s}$ (Fig 2.1.b). A resonant system may be a gluon-gluon system (gluonium, see review [7]), or a hybrid ($q\bar{q}g$), or may be a multiquark bag including s, $\bar{s}$ flavours.

At present, very little is known about the process $\bar{p}p \rightarrow \phi\phi$ on both theoretical and experimental sides. The cross sections have never been measured. Some guidance is provided by the measurement $\sigma(\bar{p}p \rightarrow K^+K^+K^-K^-) = 3.8 \pm 1.7 \mu b$ [8] at 1.9 GeV/c. This reaction is in fact dominated by the $\phi\phi$, the ϕK^+K^- and the uncorrelated 4K exclusive channels. On the other hand, the inclusive ϕ production ($\bar{p}p \rightarrow \phi + X$) at 760 MeV/c has been measured with a cross section $\sigma = 55 \pm 10 \mu b$ [9]. It is dominated by $\bar{p}p \rightarrow \phi + \pi^+\pi^-$. At 930 MeV/c, $\sigma = 50 \pm 20 \mu b$ [10].

In view of the theoretical interest, the $\phi\phi$ channel has been the focus of several recent production experiments:

− A BNL collaboration [11] has measured $\pi^- p \rightarrow \phi\phi n$ at 22 GeV/c. The $\phi\phi$ signal (4000 events) is found to be dominating the OZI-allowed $4K^{\pm}$ or ϕK^+K^- channels. The $\phi\phi$ mass spectrum is shown in Fig 2.2. From the spin analysis (up to 52 waves used with L = 3, J = 4), the authors conclude that three 2^{++} waves dominate the $\phi\phi$ channel near threshold, and claim this to be strong evidence for gluonium production. The interpretation of those broad states is controversial [7].

– The WA67 collaboration [12] recently presented their results from π^-Be → $\phi\phi$+X at 85 GeV/c. The $\phi\phi$ spectrum (≈13000 events) is shown in Fig 2.3, after subtraction of the uncorrelated ϕK^+K^- and $K^+K^+K^-K^-$ channels. The ratio $\phi\phi/(\phi K+4K)$ is of the order of 1. The authors tried to extract two broad resonances. As can be seen, there is no indication of the expected η_c at the level of 15 events/μb/Be nucleus, with a mass resolution of ±25 MeV/c^2.

– A Fermilab collaboration [13] has measured the inclusive production of A in pN → A + X, at 400 GeV/c, where A is any one of ϕK^+K^-, $\phi\pi^+\pi^-$, $\phi\phi$, or $\phi\phi K^+K^-$. Their $\phi\phi$ mass plot is shown as Fig 2.4. The presence of structure is inconclusive.

– The WA76 collaboration [14] has measured $\phi\phi$ production in the central region for the reactions π^+p → $\pi^+(K^+K^+K^-K^-)$p and pp → p$(K^+K^+K^-K^-)$p at 85 GeV/c, using the CERN Omega spectrometer. The ϕ signal is very clean. Unfortunately, the sample is small; only 26 $\phi\phi$ events survive from a sample of 138 events. Two ratios are of interest : $\sigma(\phi K^+K^-)/\sigma(\phi\phi)$ = 1.5±.6 and $\sigma(K^+K^+K^-K^-)/\sigma(\phi\phi)$ = .3±.2. The experiment emphasizes again the abundance of $\phi\phi$, and the relative experimental simplicity to observe the channel.

– DM2 [15] has measured the effective mass of the $\phi\phi$ system in the radiative decay of the J/Ψ. The result is shown Fig 2.5. The sample is too small to provide information on possible resonant structures.

What will a $\phi\phi$ mass plot in $\bar{p}p$ → $\phi\phi$ at LEAR look like? We do not know. But we believe this is a vital measurement to be made in order to understand the annihilation mechanism and in order to search for potential new states in the same mass range, which is accessible to LEAR. The current unclear experimental situation can be decisively clarified by our experiment, which features s-channel production, polarized target and high statistics.

Our intention is to measure the differential cross-section $d\sigma/d\Omega$ and polarization P at different energies E (at the same values of beam momentum as for the reaction $\bar{p}p$ → $K^0_sK^0_s$ discussed below). The initial approach will be to evaluate $\sigma(E) = \int(d\sigma/d\Omega)d\Omega$. The excellent sensitivity of the gas jet target will allow us to collect 2500 $\phi\phi$ → $4K^\pm$ events per day, assuming a $\sigma(\bar{p}p\to\phi\phi)$ = .1 μb and a 100% efficiency. This level of production must be considered a minimum in order to perform in a second step the polarization measurement. In this case the measurement of P can be considered as feasible and will have two interesting aspects :

i) – As stressed by S. Cooper [16], the exclusive reaction and the two spin directions allow partial wave analysis of the $\phi\phi$ mass plot, and $\bar{p}p$ → $\phi\phi$ is simpler than π^-p → $\phi\phi$n (BNL experiment). The polarization parameter will provide additional constraints on the partial wave analysis.

ii) – The polarization will allow us to study the correlation of the spin directions in the initial and final states, in a process involving purely gluonic intermediate states. The specific nature of the spin-spin short range interaction characteristic of vector gluon coupling to $q\bar{q}$ pairs, involves a correlation in the helicity of the $q\bar{q}$ both in the initial and final states [17].

2.2 $\bar{p}p$ → $K^0_sK^0_s$

The $\bar{p}p$ → $K^0\bar{K}^0$ reaction implies three different final state particles which are $K^0_sK^0_s$ (25%), $K^0_sK^0_\ell$ (50%) and $K^0_\ell K^0_\ell$ (25%). The channel $\bar{p}p$ → $K^0_sK^0_s$ → $\pi^+\pi^-\pi^+\pi^-$ represents 11.8% of all $K^0\bar{K}^0$ events.

The annihilation process of a $\bar{p}p$ system into a $K\bar{K}$ pair is sketched in Fig 2.6. It is a superposition of quark line rearrangement, and annihilation of $q\bar{q}$ pairs. The importance of $\bar{p}p$ annihilation into strange mesons has been discussed from a theoretical point of view at the Tignes Workshop by several authors [18]. The quark dynamics of $N\bar{N}$ annihilation have also been analysed by many authors, e.g. [19].

The series of quantum numbers accessible both to $\bar{p}p$ and $K^0_S K^0_S$ are $J^{PC} = 0^{++}, 2^{++}, 4^{++}...$ in a pure isospin system I = 1. The initial $\bar{p}p$ spin state is also constrained to have spin equal to one (S = 0 is forbidden by P and C conservation).

The value of the cross section is of the order of 1μb [20] i.e. $\approx 10^4$ events per day. It is foreseen to measure $d\sigma/d\Omega$ and P (polarization) at the same momenta as the K^+K^- annihilation measurements done by PS172. That will allow a simultaneous amplitude analysis from the two isospin coupled channels :

$\bar{p}p \rightarrow K^+K^-$ from PS 172
$\bar{p}p \rightarrow K^0_S K^0_S$ this proposal.

Whereas the $K^0_S K^0_S$ is a pure isospin I = 1 system, the K^+K^- is a mixture of I = 0 and I = 1.

Concerning spin amplitudes, scattering in these channels can be expressed in terms of two amplitudes F^{++}, F^{+-} which refer to helicity non-flip and helicity flip parts, as in $\bar{p}p \rightarrow \pi^+\pi^-$ annihilation [21]. The differential cross section and polarization are then defined as :

$$d\sigma/d\Omega = |F^{++}|^2 + |F^{+-}|^2$$
$$P = 2\mathrm{Im}\{(F^{++})(F^{+-})\}/\{|F^{++}|^2 + |F^{+-}|^2\}$$

These measurements combined with the PS172 data will provide significant insight into the annihilation mechanism of $\bar{p}p \rightarrow K\bar{K}$.

3. THE GAS JET

3.1 Molecular Hydrogen Jet

The use of converging/diverging nozzles (extensively studied at KfK [22]), has resulted in higher gas jet intensities, and hence very large luminosity in a small interaction region. The new target we propose to use at LEAR will make use, where possible, of components of the system previously operated at the ISR [23]. Its characteristics and the adaptation to the LEAR and detector environment are described in the following.

Figs.3.1 and 3.2 show a schematic view of the system. To allow for maximum acceptance of the detector, the production and the sink systems are placed at a given distance from the crossing point with the antiproton beam. The hydrogen beam is brought to the interaction region through a narrow (35mm diameter) drift tube, and removed likewise on the opposite side of the vacuum chamber.

The production system will be built using existing cryogenic and turbomolecular pumps in a slightly modified geometrical configuration, to allow clearance for the shielding wall of LEAR. We will add a third differential pumping stage built of Non Evaporable Getter (NEG) material, which will reduce the leakage of gas to the machine vacuum pipe. The sink stage will again use existing cryogenic pumps in a new arrangement, and a third differential pumping stage of NEG material, so as to minimize the flow of backstreaming gas.

In phase 1 the operating temperature of the gas injector (nozzle) will be kept at liquid nitrogen temperature, and a target density of 8.10^{13} atoms/cm^2 will be obtained at a H_2 pressure of 16 bar. The diameter of the H_2 jet is approximately 1 cm at the beam crossing point (the transverse size of the beam is typically σ < 3mm). For 10^{10} $\bar{p}$ circulating, this results in a luminosity of 2.5 10^{30} cm^{-2}s^{-1}. We point out that a similar target density can be obtained in this system for other gases. A certain reduction in density will result from the later insertion of longer drift tubes to accomodate the solenoid magnet. This will be compensated by lowering the temperature of the nozzle, thus raising the target

4.5 Trigger Counters

The outer surface of the RICH will be covered with a fine-grained array of trigger counters. Their function is to provide the Level 1 trigger (multiplicity) decision, the t = 0 point for the straw chamber TDC's and to identify out-of-time tracks caused by event overlap. In the barrel region, we will install 48 scintillators of 72 cm length, each equipped with two 1" phototubes with fast time response. The forward and backward end caps will each have 48 'pie' shaped scintillators of length 20 cm. Each one is read out with a single phototube, and digitized by a TDC and an ADC.

4.6 Triggering

The trigger scheme is summarized in Table 1. It is divided into the following levels:

i) Charged multiplicity. Here a decision is made locally at the detector that there are four charged tracks in the event. A significant improvement in the rejection power of this trigger is possible if there is a simultaneous requirement of zero photons. We will therefore probably install a simple photon veto tag around the detector. (Since this can be done at essentially no cost using existing equipment, it is not discussed elsewhere in this proposal.)

ii) Hardware $K^{\pm}/K^{0}_{s}$ identification. The $K^{\pm}$ identification is made first by a search through the RICH wires for the large pulse height hits corresponding to the track impact points. This search is aided by information from the scintillation counters, which are located immediately adjacent to the RICH MWPC. After locating the track impact points, a cluster count of struck wires is made for a distance of ± 5 cm on each side. This cluster will have many hits (up to 20 or so for π or high momentum K, and only $1-2$ wires for K below 0.62 GeV/c or a π below 0.18 GeV/c.
The trigger decision on K^{0}_{s} is based on either a multiplicity step or a track with finite impact parameter. The latter decision is made first by loading the straw chamber hit pattern into a shift register. By parallel clocking of the appropriate layers the multiple coincidences caused by tracks which successfully project back to the origin are located. The number of such tracks is then subtracted from the total track count (derived either from scintillators or from layerwise counts in the straw chambers), to give the residual count of tracks with impact parameter incompatible with the interaction volume.

iii) Parallel microprocessing. The hardware triggers will bring the trigger rate down below 1 kHz where useful parallel software processing can take place. These microprocessors will utilize more refined algorithms than the (loose) hardware triggers. Furthermore, the Si microstrip hit patterns will now participate in the impact parameter measurements.

4.7 Luminosity

We plan to monitor the LEAR luminosity by means of $\bar{p}p$ elastic scattering at wide angles into our detector. We will make a fast hardware identification of events containing two coplanar charged particles and no photons. The RICH will be used to require the tracks to be p ($\bar{p}$). The rate of these events will be recorded and a sample written to tape with a pre-scaled trigger rate of a few Hz. This sample will be subsequently analyzed to calibrate the fraction of elastic $\bar{p}p$ events in the luminosity scaler.

4. THE PHASE 1 DETECTOR

4.1 Overview

The key elements of the phase 1 detector are as follows:

– Fast (megahertz) triggering capability on $K^{\pm}$ (or $p,\bar{p}$). The physics channels of interest ($\phi\phi$ and $K^0_s K^0_s$) have cross sections in the the range $< 10\mu b$. When compared with the cross–section $\sigma(p\bar{p} \rightarrow \text{anything}) \approx 100mb$, this implies a signal-to-background ratio in unselected events of $< 10\mu b/100mb$, i.e. $< 10^{-4}$. This is an exceedingly rare signal which must be selected in the presence of a raw event rate of $L\sigma = 2.5*10^5 Hz$.

– A fast and precise tracking system which can trigger on K^0_s production by identification of either a multiplicity step or by a track with a finite impact parameter with respect to the interaction volume (length 10 mm, $\sigma_{\perp}$ = 3 mm).

– A compact geometry. The constraints of optimal gas jet operation, limited free space at the LEAR ring and the need to detect low energy $K^{\pm}$ before decaying ,all require a compact detector design.

– Good solid angle coverage, with particular attention to the forward region. At the low $\sqrt{s}$ values of LEAR a gas jet detector must cover not only the forward region (which is especially important for $\phi\phi$ production) but also a large fraction of the backward hemisphere. LEAR physics involves exclusive analysis of events and so solid angular coverage will sharply influence signal detection efficiencies and background contributions from states involving missing particles.

The design concept of our detector (Fig 4.1) fulfills these requirements as follows:

– Inner tracking system based on Si microstrip technology [27] and the straw vertex chamber design developed by HRS [28], MAC [29], and, more recently , TPC [30] at PEP.
– Fast RICH detector using a liquid C_6F_{14} radiator. The photosensitive chamber is of a new high speed design [31] involving a thin MWPC with wire and pad readout.
– Outer layer of trigger scintillators.

These components, together with the gas jet, represent the phase 1 realization of the detector. The detector has good geometrical acceptance: For the $\phi\phi \rightarrow 4K^{\pm}$ channel, 35 and 80% of events at lowest and highest beam momentum will be fully reconstructable. For the $K^0_s K^0_s$ channel, the corresponding numbers are 60 and 40%.

It is our intention to develop this core detector according to the future resources and future physics aims of our collaboration. The future phases will involve the following additional components:

i) A 6 Tesla superconducting solenoid. The small overall dimension of the detector makes practical an ultra high magnetic field. In order to accommodate the gas jet, two circular apertures of diameter 15 cm are included in the design of the cryostat (see Fig 3.1 and 3.2) and the superconducting solenoid is wound into two discrete coil assemblies.

ii) A precision electromagnetic calorimeter based on BGO crystals with photodiode readout. The array has good transverse granularity and depth segmentation ($0-5\ X_0$ and $5-16\ X_0$) by means of photodiode readout at both the front and back faces of each crystal. The energy resolution at 100 MeV is σ = 5%, and the noise is 0.8 MeV per crystal (L3 measurements). Photon positions are measured to an accuracy σ = 2mm (σ_{θ} = 7 mr) by energy sharing. The array extends to an outer radius of 44 cms, and the total volume of BGO is 430 litres.

density due both to the increase in the H_2 beam intensity and to the reduced velocity of the clusters. Two additional pumping systems built with NEG material, which are already in preparation following the design of the LEAR vacuum group, will reduce the pressure in the interaction region. Two UHV valves will separate both the production and sink stage from the LEAR vacuum pipe. As a consequence, the jet system will be **completely isolated from LEAR** when not in operation.

3.2 The Polarized Jet Target

The polarized atomic hydrogen jet target is based on a scheme that has already been developed in several laboratories, and successfully operated at CERN [24]. The principle of operation is as follows: The atomic beam is produced by hydrogen atoms expanding through an injector (nozzle) from a vessel in which H_2 gas is dissociated by a RF discharge. The maximum intensity is reached at a pressure value of the hydrogen in the vessel at which recombination of atoms is still not dominant. Intensities of the order of 10^{19} atoms/sec/steradian have already been obtained. The electronic spin separation is obtained by means of a sextupole magnet whose axis coincides with that of the expanding gas. The special configuration of the magnetic field (zero on the axis, increasing proportional to r^2 up to the pole tip) is such that states with positive electron spin component perform stable oscillations around the magnet axis, while the other atoms are defocussed and recuperated by the pumping system acting on this stage.The nuclear spin selection is obtained by means of an RF transition between hyperfine states.

A target system based on this principle is under development [25], and it will be used to optimise the parameters which are essential for the final target thickness:

i) Efficiency of dissociation, to get the largest pressure value in the dissociation chamber (maximum intensity out of the nozzle)

ii) Temperature of the expansion nozzle. This determines the velocity of the H_2 atoms (the target thickness is inversely proportional to the velocity) and the angular acceptance of the sextupole magnet;

iii) Geometry of the sextupole magnet. This determines the fraction of the expanding gas which is focussed onto the interaction region.

The aim of the optimisation is to get a target density of $1.5*10^{12}$ atoms /cm^3 in the interaction region [24]. The final production system will then be composed of three stages: dissociation stage, electron spin selection, nuclear spin selection. A pumping system with turbomolecular pumps will be acting on each of these stages in order to provide the differential pumping stages necessary to minimise the gas leakage to the LEAR beam vacuum pipe. The mechanical fittings for the sextupole and spin flip stage leave enough room to install all detector elements.

We should point out that an internal polarized atomic hydrogen jet target compares well with a conventional solid state polarized proton target. There is no complex nucleus, hence all nucleons are polarized, and no dummy target runs are needed. The polarization can be rapidly oriented in any direction, and can be flipped at high frequency. It also is intrinsically at a higher level.

The later introduction of the solenoid magnet will allow only the use of longitudinal polarization due to the presence of the strong magnetic field [26].

4.2 Silicon Microstrip Tracker

The silicon microstrip system will provide several (3 – 6) high precision (σ = 10μm) points along each track in order to allow precise vertex measurements for K^0_s identification. Information will be used both in the off-line reconstruction and also in the 3rd level on-line trigger, which refines the fast but approximate impact parameter trigger based on the straw chamber hit pattern.

In addition to providing precise tracking points, each Si layer will measure the track dE/dx to $\sigma \approx$ 20%. This information will be useful in the level 3 trigger and subsequent analysis, for flagging very soft particles. The latter present a potential problem in that they can scatter readily and create spurious impact parameters.

Silicon microstrip tracking has been used very successfully by fixed target experiments such as NA32 and WA75. These experiments provide an existence proof of the precise operation, reliablity and stability of such systems in high luminosity environments. Furthermore, impressive progress has taken place in developing the VLSI readout necessary for the large systems ($\approx$ 100 K channels) required by collider vertex detectors. The VLSI development is being carried out by the CERN – Hawaii – Stanford ('Microplex') collaboration [32] for DELPHI and Mark II and by a MPI-Munich/Dortmund collaboration for ALEPH.

With these developments Si tracking can now be viably considered by a broader group of experimental physicists. Based on our discussions with the DELPHI Si group [32] we believe the Microplex development can be applied directly to our detector. In addition to the fine track resolution, the Si microstrip wafer with Microplex readout provides many advantages such as the compact nature of the device and the readout chips, precise macroscopic structures for ease of alignment, mechanical stability and simple operation with a minimal cable plant. In fact, the major challenges now centre on mechanical aspects such as precise support structures and cooling the VLSI electronics.

Our system is based on Si wafers with thickness 280μm ($3*10^{-3} X_0$) and area 6 x 3.2cm^2. Each wafer contains 1280 strips with a spacing of 25 μm. In view of the low particle density at LEAR, only 1 out of 3 strips will be connected to the readout, the excellent position resolution being maintained by means of capacitive charge division. For example, σ = 8 μm has been measured for a device with 20 μm pitch and readout only at every sixth strip. Wafers are 'daisy-chained' in pairs and then a readout board is wire bonded to one edge. The readout board with four Microplex chips (preamplifier, sample-and-hold and multiplexer) is extremely compact: 32 x 5 mm^2 in area. The wafers are assembled into a mosaic to form the 3 z layers in the barrel region (Fig 4.2) and the 3 xy paired layers in the forward region. By slight staggering in the radial positions (or z, in the case of the forward detectors), dead spaces between chips are essentially eliminated. This mosaic structure readily accommodates the awkward geometry of the gas jet tubes and the LEAR vacuum chamber. In order to achieve the best match to this geometry we are investigating the possibility of cutting wafers. The number of wafers in the barrel is 244 and there are 186 in the forward detector. The total Si area is 0.83 m^2. There are 92K readout channels which dissipate 2.3 KWatts. The readout, which is clustered in readily accessible regions (such as the end regions of the barrel system) is cooled by tubes which contain liquid Freon flowing at a pressure below atmospheric.

The readout scheme is as follows. A charge-sensitive preamplifier on each strip stores charge continuously on a capacitor until reset. Resets occur every 4 μs unless a trigger level is satisfied. The reset period of 400 ns imposes an experiment dead time of 10%. During the 3.6 μs live period all events are integrated. If an additional event occurs in the same period, the straw tracking and scintillation counters are used to identify the in-time Si data. Immediately following a reset a 1st sample is made of the strip charge. A 2nd sample is made if a level 1 trigger is satisfied. These samples are then compared sequentially for each strip through a differential amplifier into an ADC. The readout time into a RAM is 500 μs assuming groups of 1280 channels are fed into one ADC/pedestal subtraction and compaction unit. If the level 2 trigger is not satisfied, the Si readout is aborted and a reset applied to the system.

The Si tracking system will be assembled in stages according to the rate of arrival of components. The highest priority will be given to the forward tracker, involving about 1/2 of the full system.

Finally, we note that the introduction of a magnetic field will introduce an E x B shift on the charge carriers in the Si wafers. This will be zero in the forward plane since E is parallel to B, but will cause a mean transverse shift in the barrel region of 40 μm. This effect is easily corrected (and is not subject to any statistical fluctuations since the signal charge is large: 25000 e-hole pairs). With a 6T field, the chambers will allow a precise momentum determination of $(\sigma_p/p)^2 = (0.004p\ [GeV/c])^2 + 0.01^2$.

4.3 Straw Chambers

The straw chamber system will provide the detector with a fast track finding capability. Using merely the hit pattern, the transverse accuracy is σ = 2 mm and, after processing the analogue (time and pulse height) data, the transverse measurement error is σ = 100 μm and the longitudinal error σ = 2 mm. The functions of the straw chamber are as follows:

i) To provide a fast trigger for K^0_s decays based on either changes in multiplicity inside the tracking volume or tracks with finite impact parameters relative to the interaction volume.

ii) To serve as the main component for track pattern recognition in the off-line analysis.

iii) To provide a pointer for location and association of the high precision Si track points. This feature is relevant both to level 3 on-line triggering and to precise track measurements in the off-line analysis.

We have chosen a straw drift chamber design ([28], [29], [30]) because it combines many practical advantages with excellent performance:

i) Readily adapted to awkward geometries (caused in our case by the gas jet tubes, elliptical pipes and disc-shaped forward detector).

ii) Simple to construct. The MAC chamber [29] was conceived, prototyped, constructed and successfully commissioned in less than one year.

iii) Reliable to operate. Any broken wire or discharge can be cured by disconnecting a single cell. In an open drift chamber such problems lead to failure of a much larger region.

iv) Self supporting. Each straw supports the tension of its own sense wire and so end plate material, etc., can be minimized.

v) Long chamber lifetime.

vi) Easy calibration with identical cells.

vii) Demonstrated excellent performance.

The system employs aluminized mylar straws, of diameter $\approx$ 7 mm, each containing a single resistive sense wire of diameter 20 μm. The wall thickness is 75 μm, which translates to $5*10^{-4}X_0$ per straw. The chamber will be operated at atmospheric pressure, with a gas to be chosen after suitable tests. MAC [29] achieved a resolution of σ = 100 μm using an $Ar:CO_2:CH_4$ mixture (49:50:1), at 1 atmosphere. Straw chamber tests by the TPC group [30] using dimethylether [33] at 1 atmosphere indicate a potential improvement in resolution by a factor of four or more, while maintaining the excellent chamber lifetime.

In the barrel region, the straws are arranged (Fig 4.2) into two groups of four layers with the wires running parallel to the beam axis The inner group has an azimuthal granularity of 48 and the outer group, 96. There are eight different tube diameters in order to ensure complete azimuthal coverage and an optimal staggered geometry. (By straightforward adjustment of the voltage on each layer there is an identical time-to-distance relationship for every straw). In the regions near to the vacuum chamber or the gas jet tubes, straws are omitted or half straws are used as appropriate. In the forward region, the straws are arranged in two groups of four layers each (xyxy). The granularity in each layer is approximately 50 straws and a single straw diameter of 7 mm is used throughout. The number of straws in the full system is 850 (550 in the barrel and 300 in the end caps).

Each resistive sense wire is read out into a TDC and the pulse height at each end is recorded with ADCs. In addition the straw hit pattern is parallel-loaded into shift registers to allow the fast hardware level 2 trigger decisions to be made.

The expected performance of this system is a transverse measurement accuracy (by timing) σ = 100 μm and a longitudinal measurement accuracy (by current division) of 1% of the wire length, i.e. σ = 2 mm. For fast triggering purposes, the straw hit pattern alone has a transverse accuracy σ = 2 mm. The resulting projection error to the origin is well matched to the interaction volume. As to be expected for geometries with extended cathodes, the chamber lifetimes are excellent: an integrated charge of $\approx$ 1 coulomb/cm can be accumulated before degradation (10^{14} tracks per straw at a gain of 10^5).

4.4 Fast RICH Detector

The ability to make fast trigger decisions on $K^{\pm}$ is the key to our proposed physics. These experiments are hopeless without this trigger capability. For example, a 'high statistics' in-flight experiment with 10^7 unselected events written on tape would contain $\approx$ 25 $\phi\phi \rightarrow 4\,K^{\pm}$ events assuming $\sigma(\bar{p}p \rightarrow \phi\phi)$ = 1μb and 100% efficiency; this sample is collected by our detector in less than one minute of data taking.

Of the various techniques available for separation of π/K in this energy range (< 1 GeV) we find the RICH [34] to be the only one capable of triggering at the megaherz level. We have rejected other techniques such as time-of-flight or dE/dx, which require momentum measurements and very careful system calibrations and corrections. These calculations take a long time (several 10 msec), and are moreover probably unrealistic to be tackled on-line. Our proposed RICH (Fig 4.3) is of a new high rate design [31]. The radiator is liquid Freon C_6F_{14} (n = 1.277, boiling point at atmospheric pressure 56°C). The Cerenkov thresholds in this liquid are: π (180 MeV/c), K (620 MeV/c) and p (1180 MeV/c). These thresholds are well matched to the K momentum spectrum from $\phi\phi$ decays; the device therefore operates in a straightforward threshold mode over most of the spectrum.

The new aspect involves a photosensitive chamber with much faster response than the 'standard' TPC device. It is a MWPC with CH_4 + C_2H_6 + TMAE gas, working at 70°C in order to reduce the photon mean free path to 1.5 mm. The wire spacing is 2 mm and the outer cathode plane is divided into 1 x 1 cm^2 pads to provide the ring measurement. The anode wires are 20 μm diameter. They are made either from spring-loaded tungsten wires, or from metallized quartz fibres, in order to avoid problems from differential thermal expansion. Owing to the small thickness of the gas layer and the very short photon mean free path, the ionization of charged particles crossing the detector should not cause problems and 'cloisons' [31] can be avoided.

The total thickness of the fast RICH, including pad electronics placed on the outer surface is 10 cm and the material represents $0.2X_0$. There are 1 K wires and 11 K pads. The readout involves only the addresses of wires or pads which are above a first threshold. A further bit is set if the pulse height is above a second threshold (to signal the presence of a crossing track rather than a Cerenkov photon). Based on the DELPHI measurements [31] we expect a yield of 21 pe for β = 1 tracks at normal incidence. At a steep angle, the yield reduces to one half this value.

8. SUMMARY

Our proposal addresses a fundamental physics study at LEAR which is accessible uniquely to a detector around a gas jet target. The detector which we propose to build utilizes state-of-the-art technologies to meet the experimental challenges, without relying on adventurous detector research. The detector and the gas jet target, operating with unpolarized and polarized hydrogen, can be built within the resources of our collaboration, and can be made available for running soon after ACOL comes into operation.
According to the future physics aims and resources of our collaboration, a harmonious development of the proposed detector into an advanced general-purpose detector is possible. This will be characterized by large acceptance, optimal particle identification for charged tracks, and high resolution measurements of charged and neutral particles.

9. ACKNOWLEDGEMENTS

This proposal could not have been written without the active and invaluable help of many colleagues whose knowledge and experience we were allowed to draw upon. We want to thank especially A.Penzo for his help in writing the proposal, and R.Billinge, R.Horisberger, W.Jank, W.Kubischta, P.Lefevre, E.Lorenz, D.Möhl, M.Morpurgo, F.Piuz, W.Ruckstuhl, J.Séguinot, T.Taylor, P.Weilhammer, and T.Ypsilantis for extensive discussions.

REFERENCES

[1] CERN/PSCC 86 – 10 (PSCC/M252), 22 Jan 1986

[2] M.Macri, Proceedings of the CERN Accelerator School, October 1985, CERN 85 – 15.

[3] P.Dalpiaz, Proceedings of the Joint CERN/KfK Workshop on Physics with Cooled Low Energy Antiprotons, Karlsruhe Report KfK 2836, (1979) p.111.

[4] D.Möhl, K.Kilian, p̄ LEAR note 44 (1979), and K.Kilian, Workshop on Physics at LEAR with Low Energy Cooled Antiprotons, Erice 1982, p.677 and p.701.

[5] U.Gastaldi and R.Klapisch, The LEAR Project and Physics with Low Energy p̄. Nuclei to Particles, 1981, LXXIX Corso. Soc. Italiana di Fisica, Bologna.

[6] D.Möhl, Technical Implications of Possible Future Options for LEAR. In: Physics with p̄ at LEAR in the ACOL Era, Tignes (1985) p.65.

[7] C.Heusch, Review Talk at S.Miniato (1985), SLAC PUB 3845.

[8] J.Davidson, Phys.Rev. D9 (1974) 77.

[9] S.Cooper, Nucl.Phys. B136 (1978) 365.

[10] L.R.Price, Nucl.Phys. B85 (1975) 326

[11] Etkin et al.,Phys.Rev.Lett. 49 (1982) 1620.

[12] P.S.L.Booth et al., CERN/EP 85-138

[13] D.R.Green et al., Fermilab-Pub 85/120-E

[14] T.A.Armstrong et al., Phys.Lett. 166B (1986) 245

[15] J.E.Augustin et al., LAL/85-27

[16] S.Cooper, SLAC-PUB-3819

[17] A.Penzo, Rapporteur talk at VI Int. Symposium on Polarization Phenomena in Nuclear Physics, Osaka 1985.
Y.Onel, A.Penzo, R.Rossmanith, paper submitted to Workshop on Low Energy Antiproton Facility, Fermilab, April 1986.

[18] Physics With Antiprotons at LEAR in the ACOL Era. Workshop Tignes 1985, Editions Frontières: J.G.Körner, p.209; B.Moussalam, p.203; G. Ihle et al., p.192; J.A.Niskanen, p.193; A.M.Green, p.185.

[19] C.B.Dover, BNL 36821 (1985)

[20] T.Handler et al., Nucl.Phys. B110 (1976) 173
J.Duboc et al., Nucl.Phys. B46 (1972) 429;
J.W.Chapman et al.,Nucl.Phys. B42 (1972) 1;
S.N.Ganguli et al., Nucl.Phys. B183 (1982) 295.

[21] A.A.Carter et al., Phys.Lett. 67B (1977) 117.

[22] W.Obert, Proceedings of Rarified Gas Dynamics, Cannes, France 1978.

[23] C.Baglin et al., CERN EP Report 85 – 01 (1985).

[24] I.F. Silvera et al. Phys.Rev. Lett. 37 (1976) 136
H.G.Mathews PhD thesis, Friedrich Wilhelms Universität Bonn 1979
L. Dick et al. CERN EP 80 – 92 (1980)

[25] F. Levrero et al, INFN Genoca Internal Report 86 – 1 (1986)

[26] T.O. Niinikowski et al., CERN – EP 85 – 20(1985)

[27] See, for example, the excellent review talk by C.J.S.Damerell, Proc.12th SLAC Summer Institute on Particle Physics (1984), p.43.

[28] D. Rust (HRS collaboration), Invited paper presented at the 3rd Int.Conf. on Instrumentation for Colliding Beam Physics, Novosibirsk, USSR (1984), SLAC – PUB – 3311.

[29] D. Ritson et al. (MAC Collaboration), Proc. 12th SLAC Summer Institute on Particle Physics (1984) 332.

[30] TPC Vertex Chamber Proposal TPC – LBL – 85 – 20 (Sept.1985)

[31] J. Séguinot et al., Invited paper presented at the Vienna Wire Chamber Conference (1986).

[32] J.T.Walker et al., Nucl.Inst.Meth 226 (1984) 200. Also: R. Horisberger and P. Weilhammer, private communications.

[33] F.Villa, Nucl.Inst.Meth 217 (1983) 273.

[34] J. Séguinot and T. Ypsilantis, Nucl. Instrum. Methods 142 (1977) 377.

Table 1
Triggering Scheme

Level Number	Type	Detector Component	Decision Time [μsec]	Expected Rate [Hz]	Dead Time* [%]
0	Interaction	–	–	$2.5*10^5$	–
1	Charged Muliplicity	Scintillator	0.3	10^4	8
2	Parall.Hardware:				
	$>3K^{\pm}$	RICH			
	Mult.Step	Straws	4	500	4
	Impact Parameter	Straws	(parall.)		
3	Parallel Microproceesors (Refine level 2)	RICH Straws Si Chambers	$(1-5)10^3$ /No.of Processors	< 50	< 10
4	(Event Writing)				

* In addition, there is an overall experimental dead time of $\approx 10^5$ due to periodic resets in the Si readout system.

FIGURE CAPTIONS

2.1 a) $\phi\phi$ production graph from $\bar{p}p$ annihilation
b) Formation of a resonant system in the gluon intermediate state.

2.2 Invariant mass spectrum of the $\phi\phi$ system in $\pi^- p \rightarrow \phi\phi n$ at 22 GeV/c, at BNL [11].

2.3 Invariant mass spectrum of the $\phi\phi$ system in π^-Be $\rightarrow \phi\phi + X$ at 85 GeV/c by WA67 [12].

2.4 Invariant mass spectrum of the $\phi\phi$ system in pN $\rightarrow \phi\phi + X$ at 400 GeV/c at Fermilab [13].

2.5 Invariant mass spectrum of the $\phi\phi$ system in $J/\Psi \rightarrow \gamma\phi\phi$ by DM2 [15].

2.6 Graph for $\bar{p}p \rightarrow K\bar{K}$

3.1 Gas jet assembly at LEAR (plan view). The dashed lines indicate regions which will eventually be occupied by detector components.

3.2 Elevation view of the gas jet assembly at LEAR.

4.1 Longitudinal vertical cut through the final JETSET detector. Phase 1 comprises the tracking system, the fast RICH and trigger scintillation counters.

4.2 Layout of the barrel tracking system.

4.3 Cross section through the fast RICH detector.

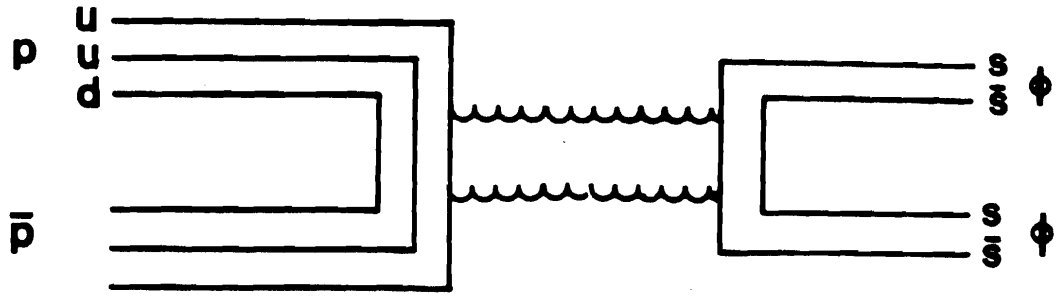

a)

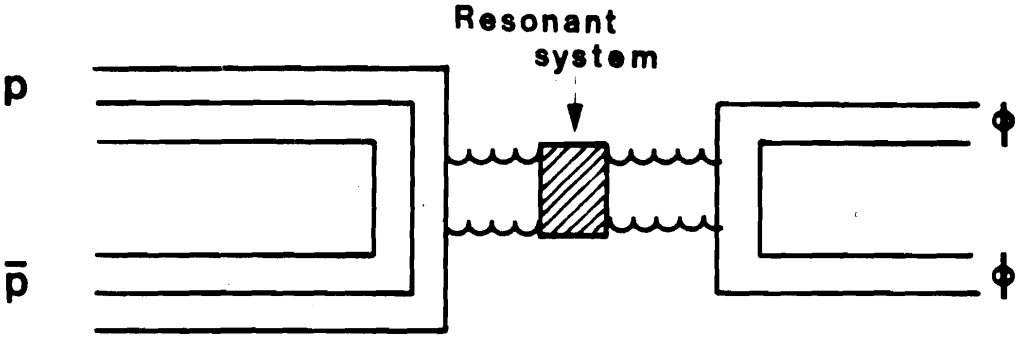

b)

Fig.2.1

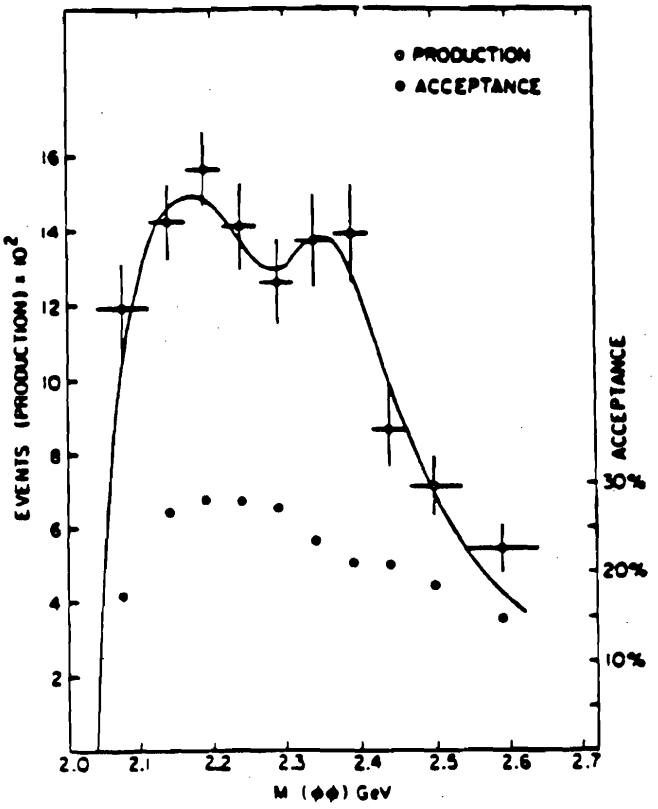
PRODUCTION
ACCEPTANCE
EVENTS (PRODUCTION) x 10²
% ACCEPTANCE
30%
20%
10%
M (φφ) GeV

Fig.2.2

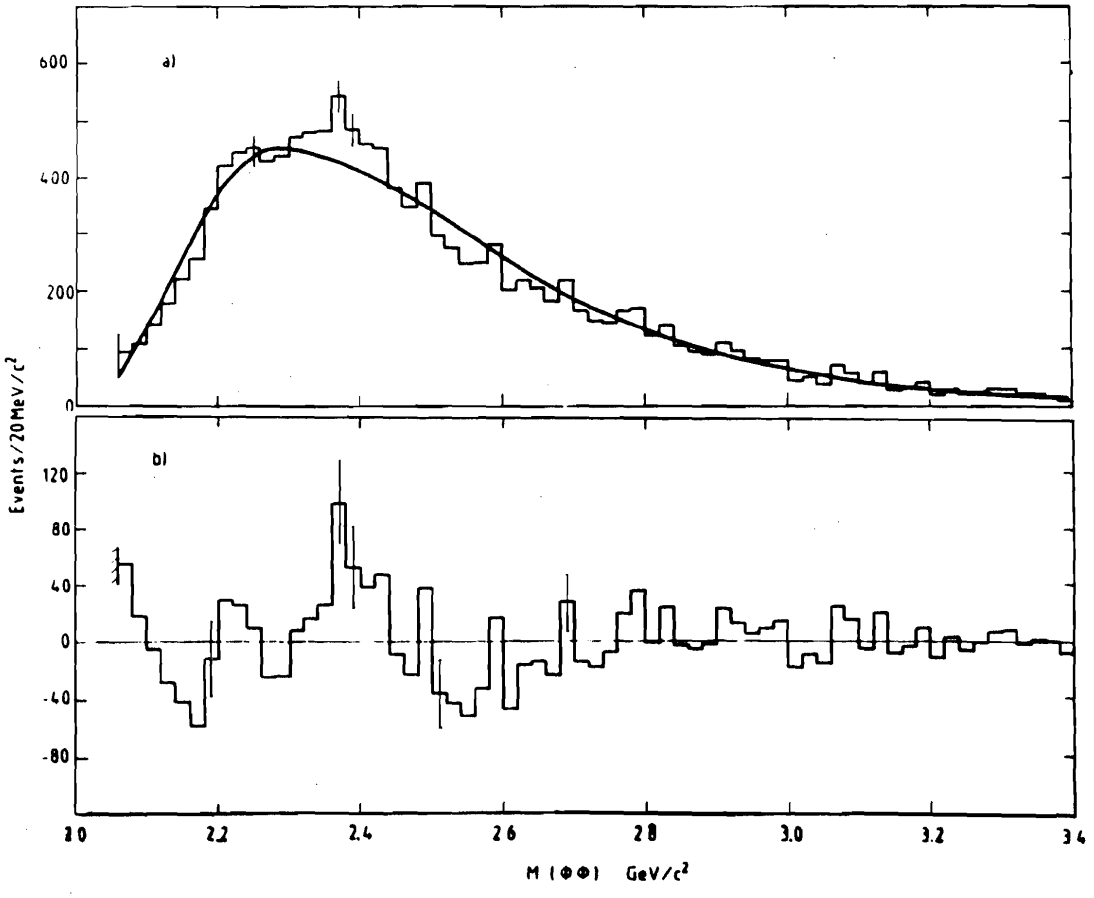
a)
b)
Events/20MeV/c²
M (ΦΦ) GeV/c²

Fig.2.3

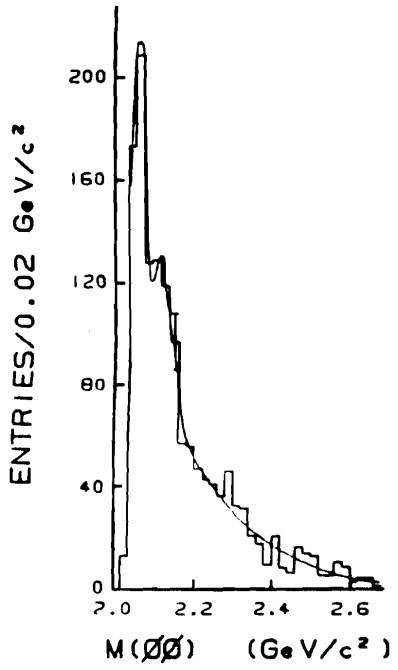
ENTRIES/0.02 GeV/c²
200
160
120
80
40
0
2.0
2.2
2.4
2.6
M(ØØ) (GeV/c²)

Fig.2.4

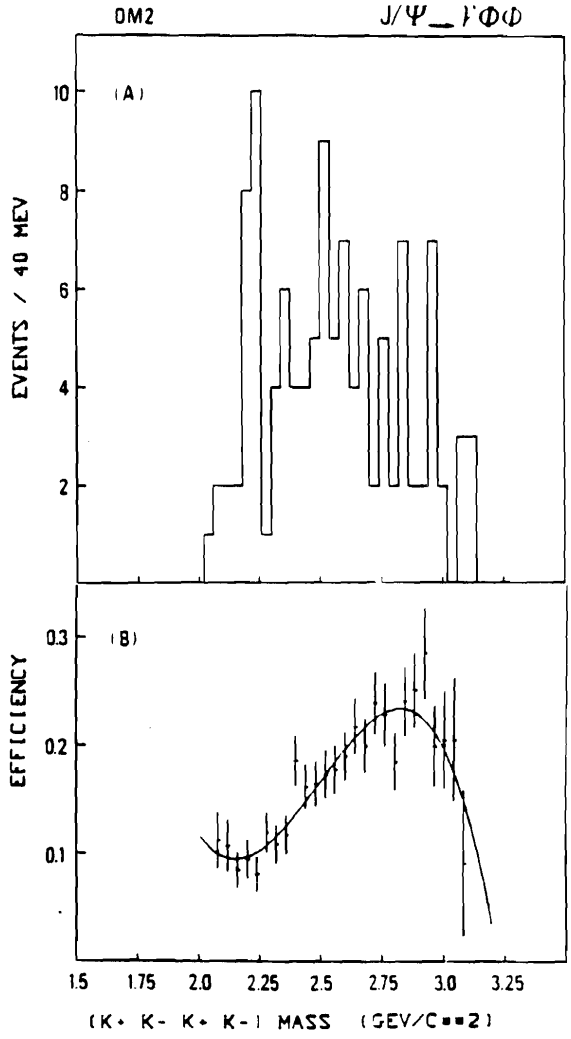
DM2
J/Ψ → ΦΦ
(A)
EVENTS / 40 MEV
10
8
6
4
2
(B)
EFFICIENCY
0.3
0.2
0.1
1.5
1.75
2.0
2.25
2.5
2.75
3.0
3.25
(K+ K- K+ K-) MASS (GEV/C**2)

Fig.2.5

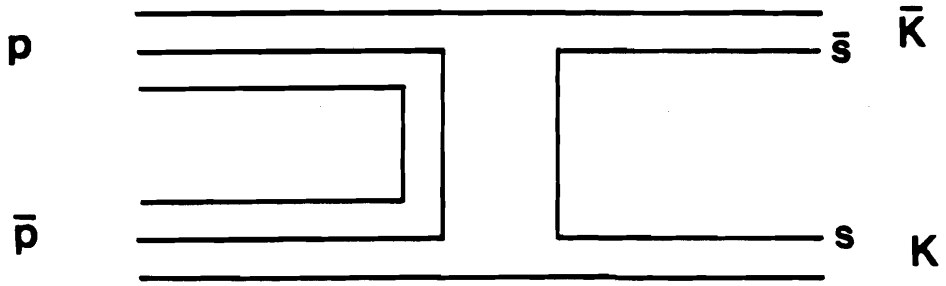

Fig.2.6

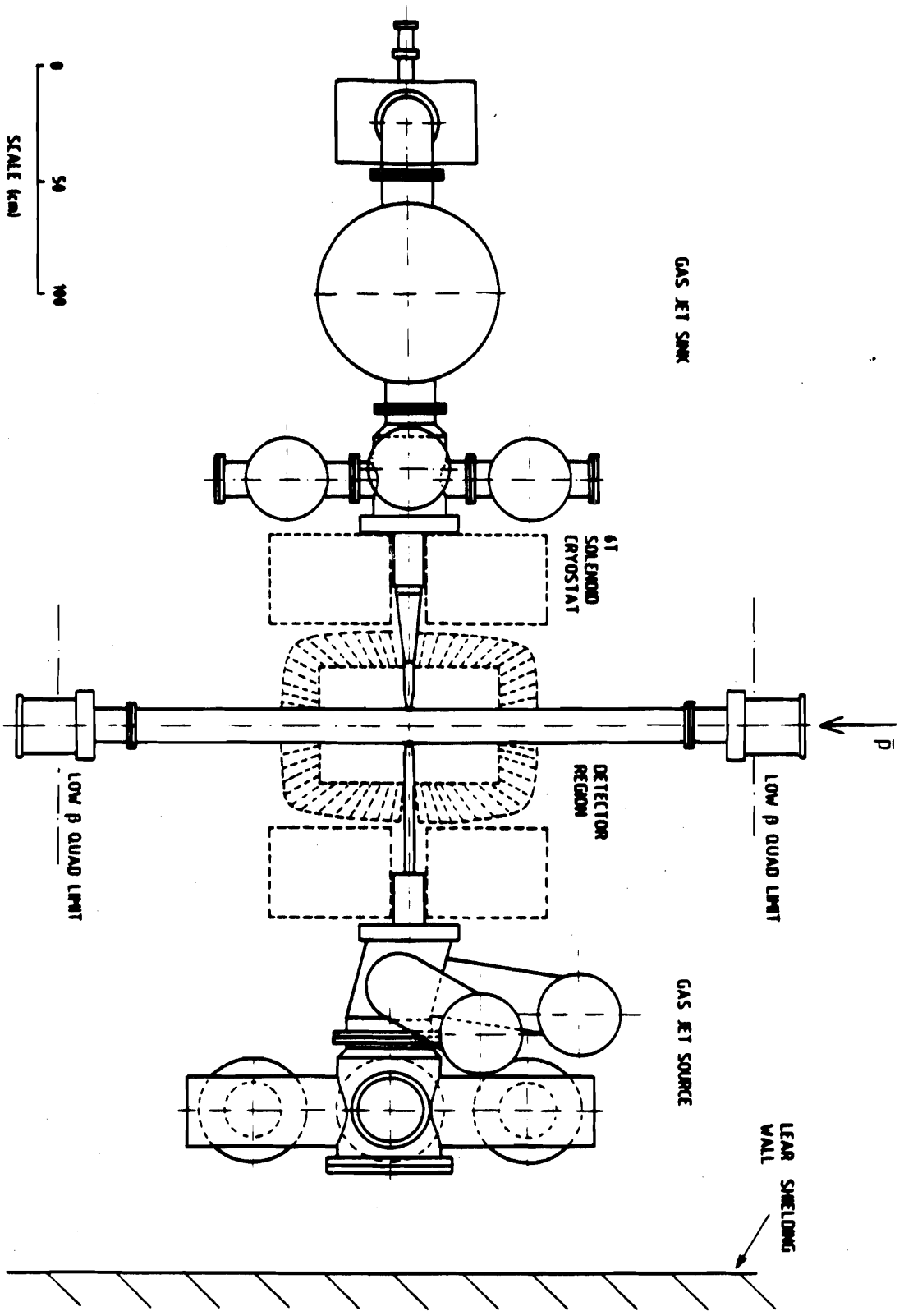
0
50
100
SCALE (cm)
GAS JET SINK
6T SOLENOID CRYOSTAT
DETECTOR REGION
LOW β QUAD LIMIT
LOW β QUAD LIMIT
p̄
GAS JET SOURCE
LEAD SHIELDING WALL

Fig.3.1

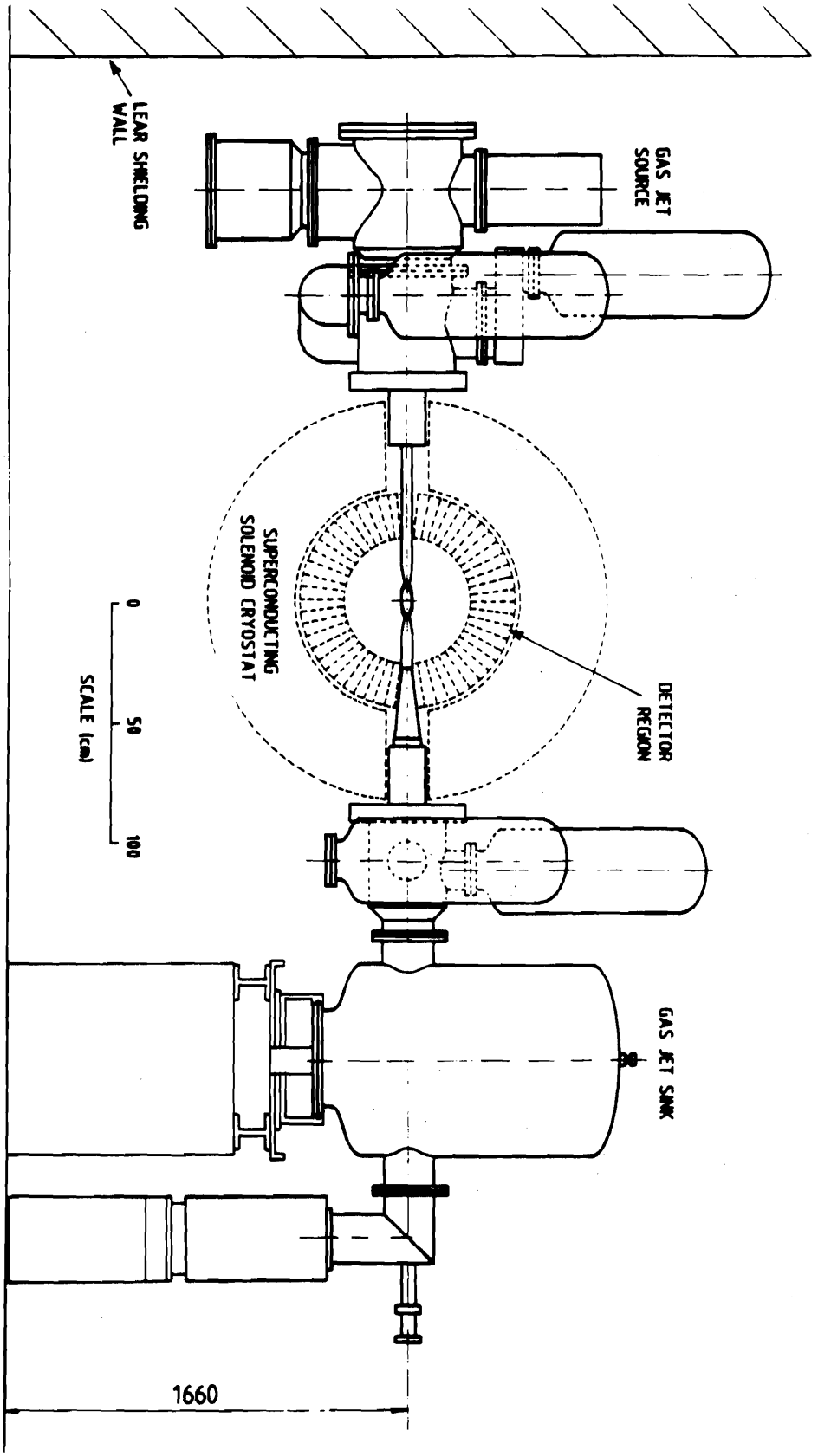
LEAD SHIELDING WALL
GAS JET SOURCE
SUPERCONDUCTING SOLENOID CRYOSTAT
DETECTOR REGION
GAS JET SINK
0
50
100
SCALE (cm)
1660

Fig. 3.2

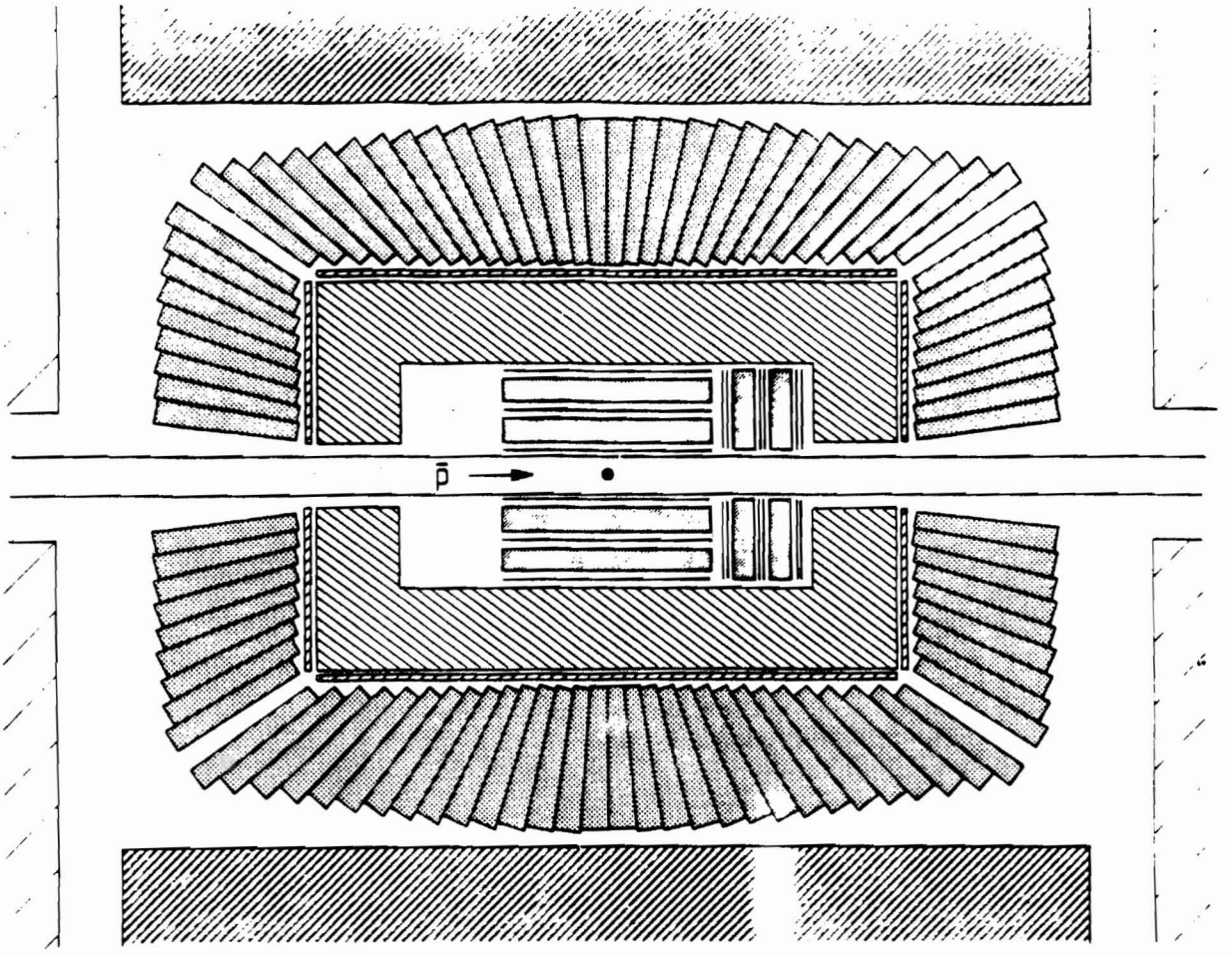

GAS JET (direction into paper)

SILICON MICRO-STRIP TRACKER (barrel: 3 z layers; end-cap: 3 x+y layers)

STRAW CHAMBER (barrel: 8 z layers; end-cap: 4 x+y layers)

FAST RICH (liquid C_6F_{14} radiator)

BGO ELECTROMAGNETIC CALORIMETER (photodiode readout)

SUPERCONDUCTING SOLENOID (6 Tesla)

FLUX RETURN (restricted to top and bottom sides of detector)

TRIGGER SCINTILLATION COUNTERS

Fig.4.1

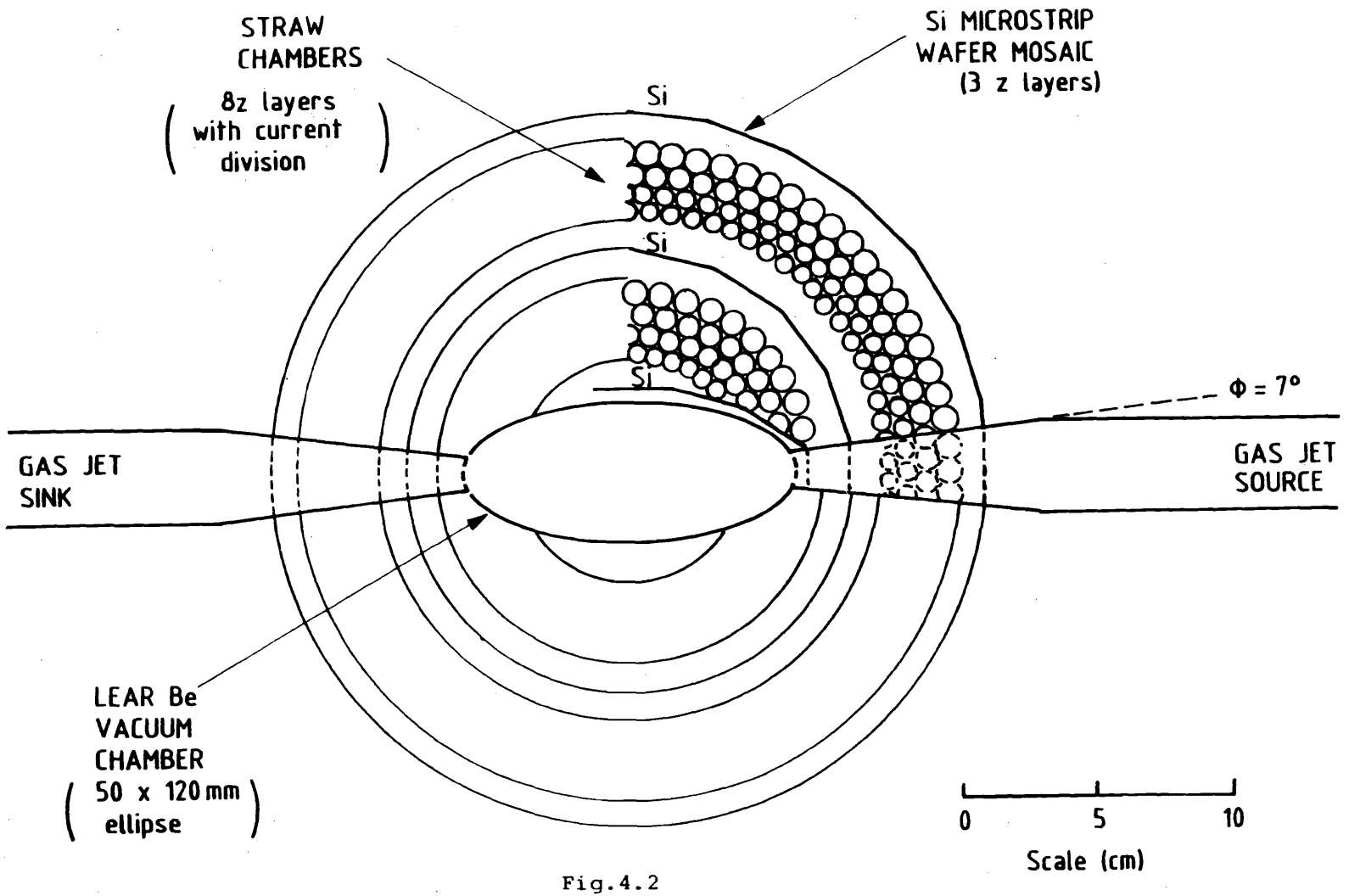
STRAW
CHAMBERS
8z layers
with current
division
Si MICROSTRIP
WAFER MOSAIC
(3 z layers)
Si
Si
Si
Φ = 7°
GAS JET
SINK
GAS JET
SOURCE
LEAR Be
VACUUM
CHAMBER
50 x 120 mm
ellipse
0
5
10
Scale (cm)

Fig.4.2

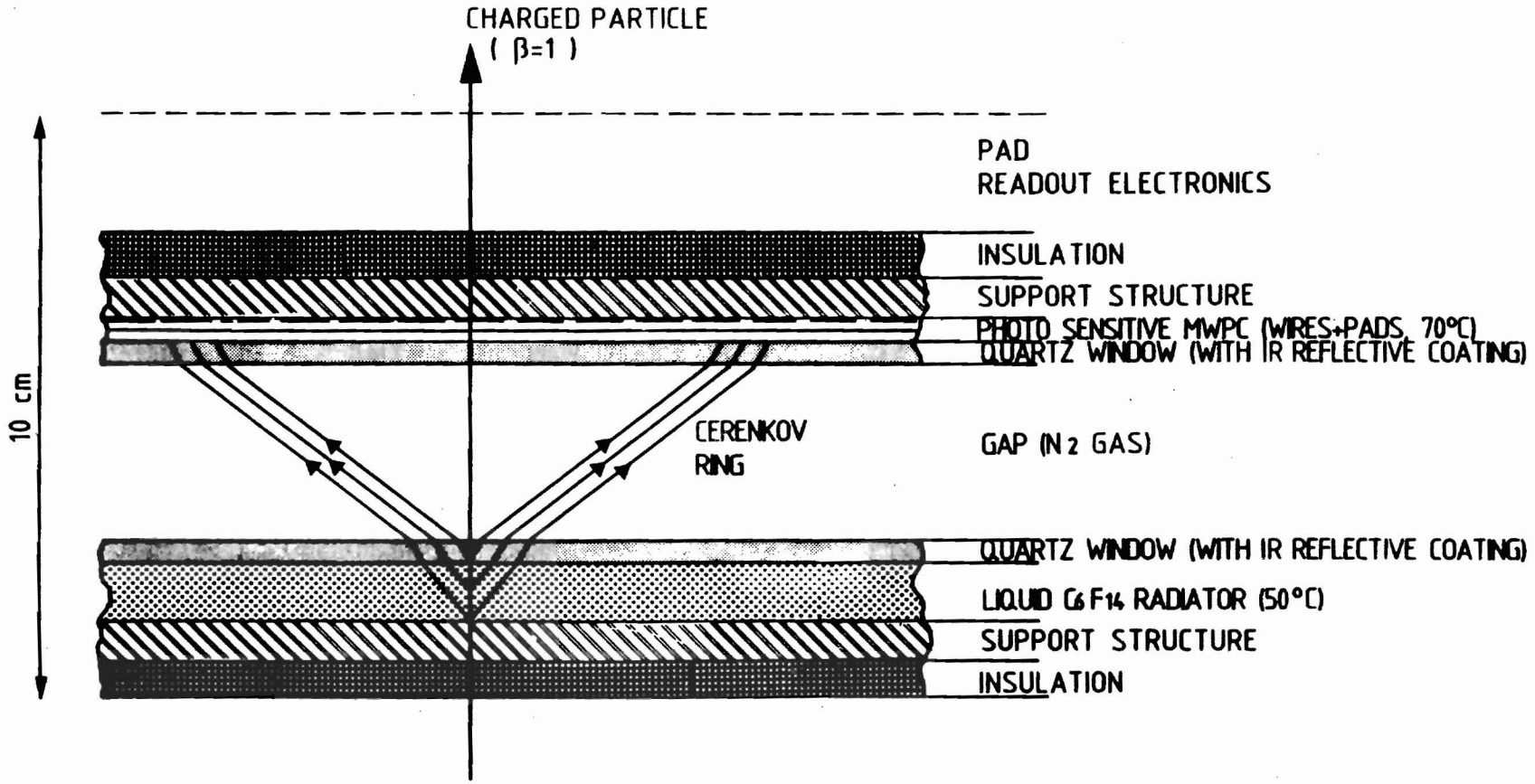
CHARGED PARTICLE
(β=1)
10 cm
PAD
READOUT ELECTRONICS
INSULATION
SUPPORT STRUCTURE
PHOTO SENSITIVE MWPC (WIRES+PADS, 70°C)
QUARTZ WINDOW (WITH IR REFLECTIVE COATING)
CERENKOV
RING
GAP (N2 GAS)
QUARTZ WINDOW (WITH IR REFLECTIVE COATING)
LIQUID C6F14 RADIATOR (50°C)
SUPPORT STRUCTURE
INSULATION

Fig.4.3